Available online at www.sciencedirect.com
SCIENCE DIRECT
Journal of volcanology and geothermal research
ELSEVIER
Journal of Volcanology and Geothermal Research 153 (2006) 97–111
www.elsevier.com/locate/jvolgeores

DEVIN: A forecasting approach using stochastic methods applied to the Soufrière Hills Volcano

Olivier Jaquet [a,*], Roberto Carniel [b], Steve Sparks [c], Glenn Thompson [d], Rabah Namar [a], Mauro Di Cecca [b]

[a] *Colenco Power Engineering Ltd, Täfernstr. 26, 5405 Baden, Switzerland*
[b] *Dipartimento di Georisorse e Territorio, Università di Udine, Italy*
[c] *Department of Earth Sciences, Bristol University, UK*
[d] *Montserrat Volcano Observatory, Montserrat, BWI, and British Geological Survey, UK*

Received 1 June 2004; accepted 18 August 2005
Available online 5 January 2006

Abstract

Time series recorded at active volcanoes are often incomplete and can consist of small data sets. Due to the complexity of volcanic processes and inherent uncertainty, a probabilistic framework is needed for forecasting. A stochastic approach, named DEVIN, was developed to perform forecasts of volcanic activity. DEVIN is a multivariate approach based on geostatistical concepts which enables: (1) detection and quantification of time correlation using variograms, (2) identification of precursors by parameter monitoring and (3) forecasting of specific volcanic events by Monte Carlo methods. The DEVIN approach was applied using seismic data monitored from the Soufrière Hills Volcano (Montserrat). Forecasts were produced for the onset of dome growth with the help of potential precursors identified by monitoring of variogram parameters. Using stochastic simulations of plausible eruptive scenarios, these forecasts were expressed in terms of probability of occurrence. They constitute valuable input data as required by probabilistic risk assessments.

Keywords: Soufrière Hills; dome growth; time series; variogram; memory effects; stochastic modelling; forecasting

1. Introduction

Several authors have proposed forecasting approaches using increases in seismicity (Kilburn and Voight, 1998; Kilburn, 2003; Ortiz et al., 2003) and ground deformation (Voight et al., 1998) as well as integrated approaches (Voight et al., 2000). These models enable forecasts of eruptive events at short term (days to weeks). These deterministically based models do not integrate aleatory and epistemic uncertainty (Woo, 1999) when forecasting volcanic eruptions. Uncertainty is mainly related to imperfect knowledge of non-linear physical process inherent to volcanic activity and to limited amount of monitoring information. Therefore, a probabilistic formalism is commonly required for the forecasting of volcanic eruptions (Sparks, 2003). One example is the Event Tree approach (e.g., Newhall and Hoblitt, 2002), recently implemented and applied to Vesuvius (Marzocchi et al., 2004). The importance of the use of multivariate data has also been recently recognized (e.g., Jaquet and Carniel, 2003), also with complemen-

* Corresponding author. Tel.: +41 56 483 1576; fax: +41 56 483 1881.
E-mail address: olivier.jaquet@colenco.ch (O. Jaquet).

0377-0273/$ - see front matter © 2005 Elsevier B.V. All rights reserved.
doi:10.1016/j.jvolgeores.2005.08.013

tary approaches like pattern recognition (e.g., Sandri et al., 2004).

The monitoring of active volcanoes using automatic recording devices is particularly prone to data losses because of hazardous geological conditions encountered in situ. However, most statistical methods applied to the investigation of short to medium term volcano dynamics require time series with fairly large data sets without gaps in the observations.

In order to take account of uncertainty and small data sets (with gaps), a stochastic approach, named DEVIN (*D*educing *E*ruption of *V*olcanoes *I*n the *N*ear future), aiming at forecasting volcanic activity was developed within the framework of the EU-project MULTIMO (multi-disciplinary monitoring, modelling and forecasting of volcanic hazard). DEVIN is a multivariate approach, based on geostatistical concepts (Chilès and Delfiner, 1999), which enables characterisation in the time domain of the behaviour for multiparametric (incomplete) time series sampled at active volcanoes. Furthermore, the DEVIN approach can provide insight into natural processes involved in volcanic eruptions. By using specific statistical tools, one can detect correlation and cross correlation in time and estimate time scales at which volcanic processes are likely to occur. Such processes exhibiting memory of their past activity can be linked to volcano dynamics and foster conceptual advances which can be analysed by numerical modelling of volcanic eruptions (Melnik and Sparks, 2002).

First the theoretical concepts of the DEVIN approach are presented, followed by an application using data from the Soufrière Hills Volcano, located on the island of Montserrat (West Indies).

2. The DEVIN approach

With the aim of forecasting volcanic eruptions, DEVIN includes the following stages: (a) detection of correlation, (b) modelling of correlation, (c) identification of precursors and (d) stochastic forecasting.

2.1. Detection of correlation

Occurrences of volcanic activity are often clustered in time; i.e., volcanic events seem not to occur at random, but rather suggest behaviour correlated in time. The variogram is a statistical tool allowing the detection and quantification of time correlation. The variogram, popularized in Geostatistics by Matheron (1962), was mainly applied to spatial problems. Jaquet and Carniel (2001, 2003) have shown the capabilities of variogram analysis for time series sampled at active volcanoes.

The time series is interpreted as a realisation of a stochastic process, $V_i(t)$. Under the hypothesis of stationarity, the stochastic process is characterised by its covariance $C_{ii}(\tau)$:

$$C_{ii}(\tau) = E[(V_i(t) - m_i)(V_i(t+\tau) - m_i)]$$

where τ is the time interval, m_i is the mean of $V_i(t)$ and $E[]$ is the mathematical expectation. In comparison to the covariance, the variogram only requires the stationarity of the increments of the stochastic process, allowing a larger class of time behaviours to be described. Under this hypothesis of translation invariance, the so-called intrinsic hypothesis, the variogram $\gamma_{ii}(\tau)$ is defined:

$$\gamma_{ii}(\tau) = \frac{1}{2}E\left[(V_i(t+\tau) - V_i(t))^2\right]$$

If the variogram is bounded, it can be derived from the covariance $C_{ii}(\tau)$:

$$\gamma_{ii}(\tau) = C_{ii}(0) - C_{ii}(\tau)$$

In the multivariate case, when K intrinsic stochastic processes are under consideration, the detection and quantification of cross correlation in time is performed using the cross variogram $\gamma_{ij}(\tau)$, (Matheron, 1965):

$$\gamma_{ij}(\tau) = \frac{1}{2}E\left[(V_i(t+\tau) - V_i(t))\left(V_j(t+\tau) - V_j(t)\right)\right]$$

where $V_i(t)$, $V_j(t)$ are stochastic processes ($i, j = 1, \ldots, K$). And similarly, when all the variograms are bounded, the cross covariance $C_{ij}(\tau)$ is expressed as follows:

$$C_{ij}(\tau) = E\left[(V_i(t) - m_i)\left(V_j(t+\tau) - m_j\right)\right]$$

where m_i, m_j are the means of $V_i(t)$, $V_j(t)$.

The computation of variogram and cross variogram is carried out from the time series using the following expression:

$$\gamma^*_{ij}(\tau) = \frac{1}{2n_\tau}\sum_{\alpha=1}^{n_\tau}(V_i(t_\alpha+\tau) - V_i(t_\alpha))\left(V_j(t_\alpha+\tau) - V_j(t_\alpha)\right)$$

where $\gamma^*_{ij}(\tau)$ is the sample cross variogram and n_τ the number of data pairs separated by a given time interval. In case of irregular sampling interval or gaps in the time series, the time interval is defined according to classes.

Assuming correlation or cross correlation exist, variogram and cross variograms allows quantifying the scale at which these correlations occur in the time

domain. These correspond in fact to the memory (or persistence) of the past activity for the studied time series. For forecasting purposes, time series are required to exhibit persistent behaviour to be able to provide potential precursors.

2.2. Modelling of correlation

Once the sample variogram is computed from the data, a variogram model is fitted to the sample variogram in order to parameterise the observed behaviour (Jaquet and Carniel, 2001). Mathematical properties must be fulfilled in order to consider functions as variogram model (Chilès and Delfiner, 1999). Among the available models, the following one enables the description of the behaviour for time series sampled at active volcanoes:

$$\gamma_M(\tau) = b_0 + b_1\left[\frac{3}{2}\frac{\tau}{a} - \frac{1}{2}\frac{\tau^3}{a^3}\right] \quad \tau \le a$$

$$\gamma_M(\tau) = b_0 + b_1 \quad \tau > a$$

where $\gamma_M(\tau)$ is a model composed of a spherical variogram with a discontinuity at the origin. The parameter b_0 represents the intensity of the random component of the time series. This component is mainly related to variability occurring below the sampling scale and to measurement errors. The parameter b_1 corresponds to the intensity of the stochastic component for the time series. Finally the parameter a is the time scale which quantifies the persistence of the time series. Beyond this time scale, the behaviour of the time series becomes uncorrelated in time.

2.3. Identification of precursors

Time series with persistent behaviour represent potential precursors. The evaluation of the forecasting capabilities of these time series can be achieved by parameter monitoring. It consists in identifying variogram parameters which time behaviour is likely to be precursory in relation to eruptive events. For a time series, $V_i(t_\alpha)$, sampled at point t_α ($\alpha = 1,\ldots, N$), parameters presenting potential as precursors of volcanic activity can be estimated using a moving window approach as follows:

$$B^{w_\alpha} = \frac{b_1^{w_\alpha}}{b_0^{w_\alpha} + b_1^{w_\alpha}} \qquad \text{with } w_\alpha = t_\alpha + \frac{L}{2},$$
$$\alpha = 1, \ldots, N - L$$
$$G^{w_\alpha} = \int_{L\cdot\Delta t} \gamma^{w_\alpha}(\tau)\mathrm{d}\tau$$

where w_α is the time for the moving window and $L \cdot \Delta t$ its size. The parameter B specifies the relative intensity of the stochastic components. This parameter varies between 0 (random behaviour without memory) and 1 (persistent behaviour with memory). The parameter G, integrating the total intensity (random and stochastic) and the persistence for the time series, delivers a measure of the overall variability at the window scale.

In the presence of stationary stochastic processes, the monitoring of potential delay effects offers precursory potential. This parameter, corresponding to a shift in time of the maximum correlation between two stochastic processes, can be estimated using the asymmetrical behaviour with respect to the origin of the cross covariance (Wackernagel, 2003; Jaquet and Carniel, 2001).

2.4. Stochastic forecasting

Parameter monitoring could be applied for forecasting, but no uncertainty can be associated with such forecasts. Therefore, on the basis of precursory behaviour identification, the likelihood for the evolution of the time series is desired at short to medium term. The realisation of such forecasts (with uncertainty) requires the use of stochastic simulation on the basis of potential evolution scenarios. The chosen stochastic simulation method starts from the following decomposition (Chilès and Delfiner, 1999):

$$V_i(t_0) = V_i^*(t_0) + \left[V_i(t_0) - V_i^*(t_0)\right]$$

where $V_i{*}(t_0)$ is the kriging estimator (Wackernagel, 2003) at time t_0 using the data $V_i(t_\alpha)$ and the term $[V_i(t_0) - V_i{*}(t_0)]$ is the kriging error. Since the true value, $V_i(t_0)$, is unknown, one considers the same equation expressed in terms of simulation:

$$V_i^s(t_0) = V_i^{s^*}(t_0) + \left[V_i^s(t_0) - V_i^{s^*}(t_0)\right]$$

where $V_i^s(t_0)$ is the simulation of $V_i(t_0)$ and $V_i^{s*}(t_0)$ is the kriging estimator using only the simulated values at the points t_α; then the kriging error is replaced by its simulation:

$$V_i^{cs}(t_0) = V_i^*(t_0) + \left[V_i^s(t_0) - V_i^{s^*}(t_0)\right]$$

where $V_i^{cs}(t_0)$ is the conditional simulation. This method allows generating simulations that honour the data points of the time series. This conditioning property is important when performing simulation of the future behaviour of the time series; i.e., the simulation, starting off at the last data point available for the time series, allows inte-

gration of the latest characteristics of the data. A dilution method (Lantuéjoul, 2002) is applied for the (non-conditional) simulation, $V_i^s(t_0)$. Based on this method, simulations of a Gaussian stochastic process are produced with a spherical variogram. Since the data are usually not Gaussian, simulations matching the observed histogram are obtained using a Gaussian (bijective) transformation (Wackernagel, 2003) applied to the time series.

Potential scenarios for the evolution of volcanic activity can be considered using the following expansion:

$$V_i^{cs}(t_0) = m_i(t_0) + V_{i,r}^*(t_0) + \left[V_{i,r}^s(t_0) - V_{i,r}^{s*}(t_0)\right]$$

where $m_i(t)=E[V_i(t)]$ is the deterministic drift which form is assumed (arbitrary) polynomial and the $V_{i,r}$ correspond to residuals with zero mean. The drift becomes time dependent solely when performing forecasts. This possibility allows the introduction of external knowledge for performing sensitivity studies with respect to various scenarios of volcanic activity.

The likelihood of volcanic activity is assessed by analysing the tendency of stochastic simulations of time series to exceed given thresholds. Using a Monte Carlo approach allows performing a large number of simulations in order to estimate probability of threshold exceedance for a given future period. These estimates are interpreted as forecasts (with uncertainty) of eruptive scenarios for the selected period. These forecasts constitute valuable input as needed for probabilistic risk assessments.

3. Soufrière Hills Volcano

3.1. Seismic data

The Soufrière Hills eruption began in July 1995 and continues to the time of writing (November 2004). The MVO (Montserrat Volcano Observatory) digital seismic network was installed in October 1996 (see Fig. 1), and uses a mixture of broadband and short-period seismometers, and 24-bit digital telemetry, providing a high dynamic range of 100 dB for the short period and 144 dB for the broadband sensors. Both continuous and triggered event data are recorded with a sampling rate of 75 Hz. The broadband sensors are Guralp CMG-40T, with a corner frequency of 0.033 Hz (30 s), while the short period sensors are Integra LA-100, with a corner frequency of 0.5 Hz.

The event parameters used include:

- The time the event triggered the acquisition system (T).
- The classification assigned by a human analyst (C).
- The peak amplitude of the event (A).
- The cumulative energy (E).
- The dominant frequency (F).
- The pseudo-magnitude (M).

Both the beginning and the end of each triggered event are determined by the triggering software; 10-s pre-trigger and post-trigger windows are added to each. Events are then manually classified (C) into the following categories: volcano-tectonic earthquake, long-period earthquake, hybrid earthquake or rockfall signal (Miller et al., 1998).

The signals are then deconvolved to remove the frequency response of each instrument and high-pass filtered at 0.5 Hz to minimize ocean micro-seismic noise (which tends to dominate the broadband components). Other event parameters are automatically calculated. Peak amplitude (A), cumulative energy (E) and dominant frequency (F) are measured on each seismic component. A is the peak amplitude expressed in m/s. E is computed by summing up the squared seismic amplitudes over the duration of the signal. F is the dominant frequency, i.e., the frequency at which the peak of the ground velocity amplitude spectrum occurs.

The energy, E, of a seismic signal varies over a few orders of magnitude. It is therefore convenient to introduce a pseudo-magnitude (M), which is also determined for each event, and is proportional to the logarithm of the seismic energy measured at the vertical component of the Windy Hill (MBWH) station (Fig. 1):

$$M = a_s + b_s \log(E)$$

This single-component short-period station has had the least amount of downtime since October 1996 (many other stations were destroyed by volcanic activity). Moreover, waveforms are usually seen most clearly on this station (it is the best station for manual classification), as signal to noise ratio is high. The scale has been calibrated by fitting parameters a_s and b_s for a small number of relatively large events (mostly recorded in 1997) against the magnitude scale that the Seismic Research Unit uses for regional earthquakes.

However, it is a pseudo-magnitude scale, since in general the volcanic events cannot be located, and instead a location at sea-level directly beneath the dome is assumed. Moreover, it is applied to rockfall signals as well as to volcanic earthquakes (reasonable, since we are just comparing recorded seismic energy). On this scale, the detection magnitude is around 0.5, and the largest volcanic events recorded (hybrid earthquakes in 1997) have a magnitude of around

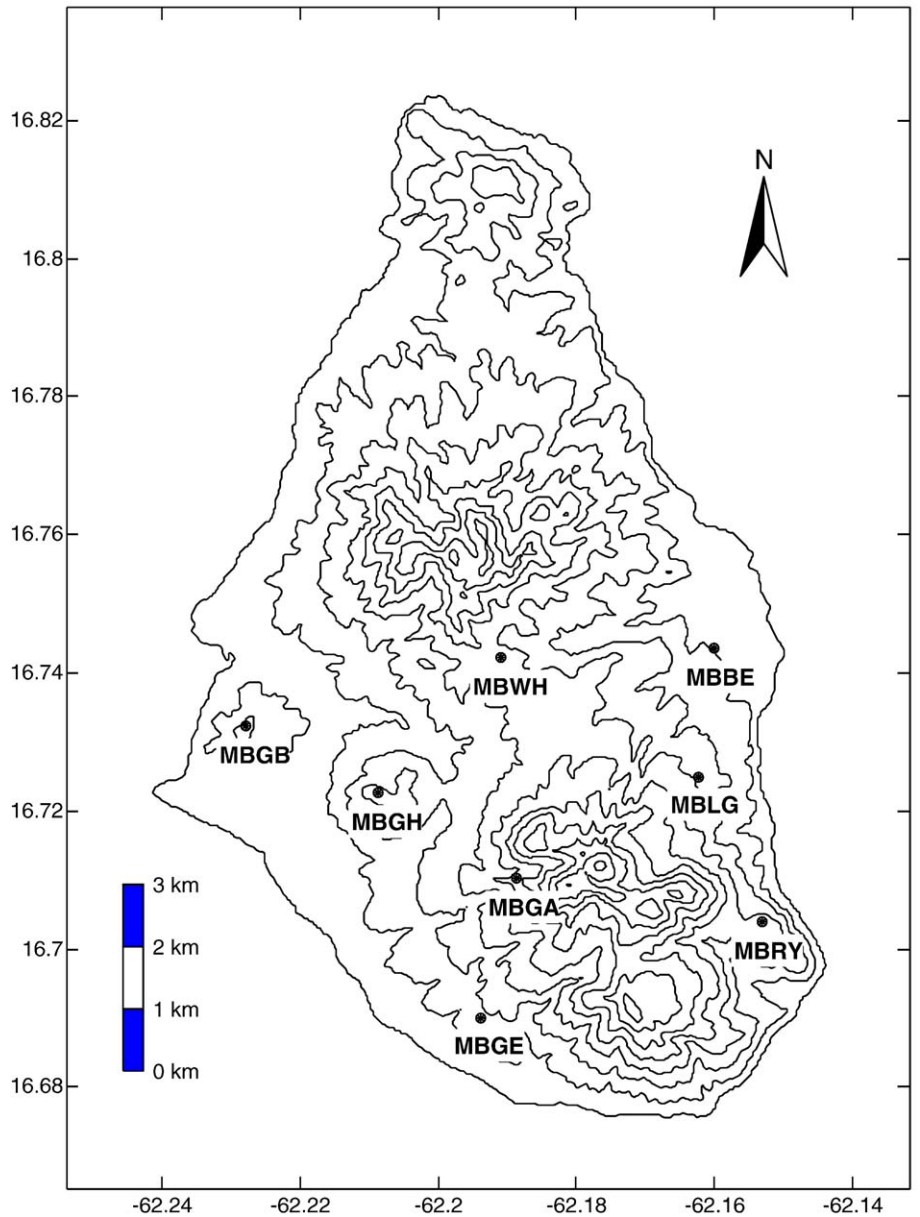

Fig. 1. Island of Montserrat (West Indies) showing the location of stations of the MVO digital seismic network, as it was originally configured in late 1996.

3.5. MBWH is a particularly useful station for this magnitude scale since it is sufficiently far from the volcano (3.6 km) that even a variation of 0.6 km in the source of volcanic events would produce magnitude variations of less than ± 0.2. Notwithstanding its simplicity, this scale has been useful to MVO to compare big single events to, for example, less significant weak earthquake swarms that would have appeared in reverse order of importance with a simple counting procedure.

The activity each day can then be summarized by the total number of events (of each type), and the cumulative energy of those events, which again can be expressed as a cumulative magnitude (of course, magnitudes cannot be summed directly since they are logarithms; it is E that is summed, and then converted to a cumulative magnitude using the equation above). This allows MVO to say that on a particular day there were 30 long-period earthquake events, and that the seismic energy of those events

was equivalent to a single *M* 2.0 earthquake (for example).

For this study, the following time series were selected for the period from 1 November 1996 to 28 February 2003 (see Fig. 2):

- Number of volcano-tectonic earthquakes per day (VT).
- Number of hybrid earthquakes per day (*H*).
- Number of long-period earthquakes per day (LP).
- Number of rockfall signals per day (RF).
- Daily cumulative magnitude for volcano-tectonic earthquakes (VT_cm).
- Daily cumulative magnitude for hybrid earthquakes (H_cm).
- Daily cumulative magnitude for long-period earthquakes (LP_cm).
- Daily cumulative magnitude for rockfall signals (RF_cm).

3.2. Volcanic activity

The Soufrière Hills eruption can be divided into several stages (Robertson et al., 2000; Sparks and Young, 2002). The first stage involved phreatic explosive activity between July and November 1995. The andesite dome appeared in mid-November 1995 and growth continued nearly continuously until March 1998 in the first major stage of dome growth. Our dataset includes part of this dome growth stage from 1 November 1996 to 9 March 1998 (Fig. 2). A stage of dome dormancy occurred between 10 March 1998 and 26 November 1999. A second stage of dome growth then started and then finished on 13 July 2003 when

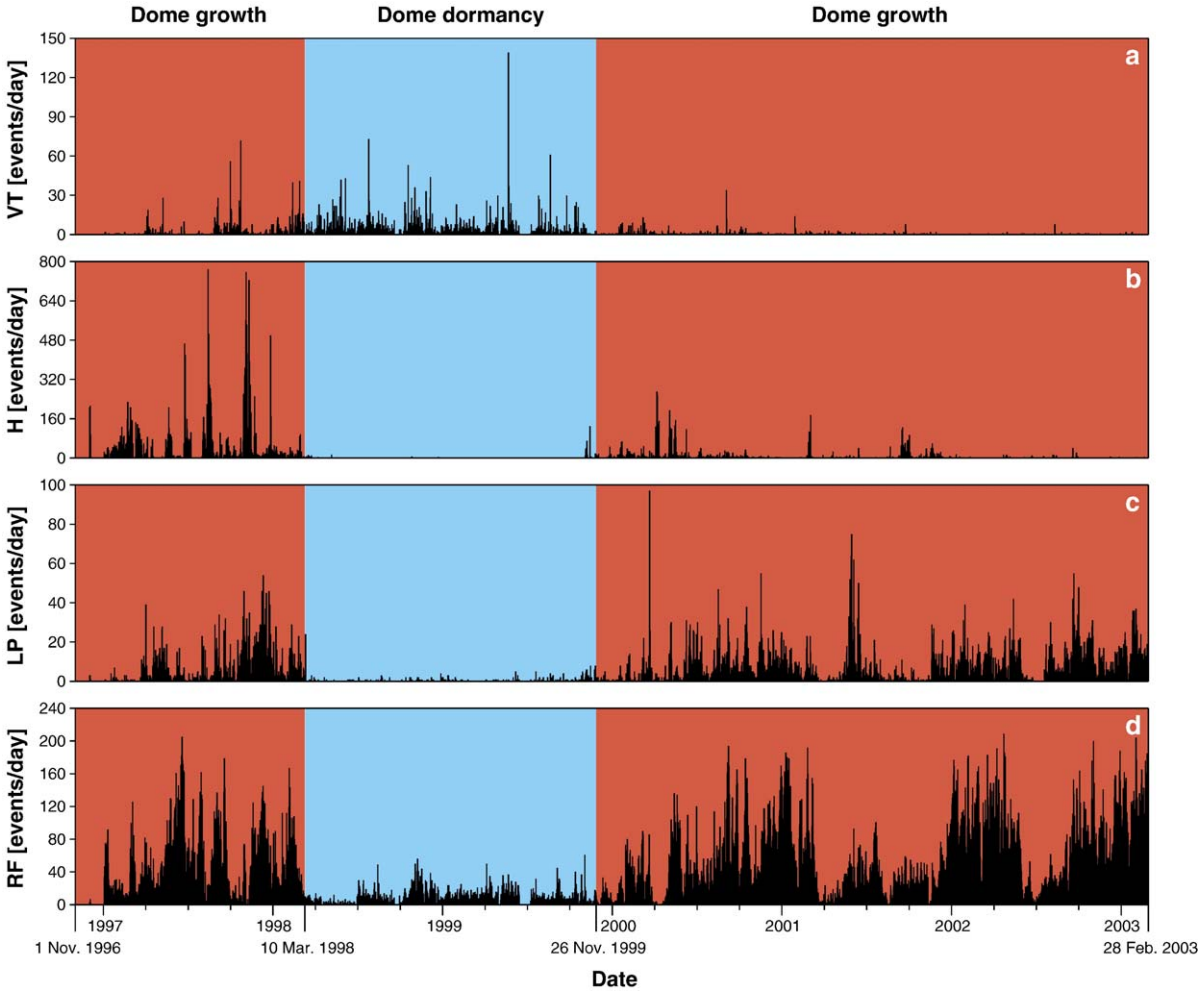

Fig. 2. Time series of volcano-tectonic (a), hybrid (b) and long-period earthquakes (c), and rockfall signals (d).

the volcano moved into a second period of dome dormancy accompanied by minor unrest. Our dataset (Fig. 2) also captures most of the second dome growth stage.

We now describe the dataset as it relates to the major features of the activity in each of the stages. This description provides some rationales for dividing the dataset into time slices, which might relate to coherent behaviour suitable for time series analysis. In the context of the dataset the different seismic events can be attributed to different aspects of volcanic activity. Volcano-tectonic earthquakes (VT's) appear in general to reflect deeper disturbances in the plumbing system. VT's have been absent or at a very low rate during dome growth, although short bursts of high rates of VT's can occur, rarely lasting more than a few days. In many cases the bursts of VT activity can be linked with some significant volcanic phenomenon, such as a major dome collapse or a new surge in extrusion rate. Notably VT activity is most pronounced in our dataset in the stage of dome dormancy. Hybrid (H) and long-period (LP) events are characteristic of dome growth. In our dataset hybrid events dominated the first stage of dome growth, long-period events were more prominent in the second period of dome growth, and long-period events were dominant in the period of dome dormancy, albeit at a much lower rate than in periods of dome growth. These relationships could be potentially affected by the manual classification procedure applied in relation with changes and/or errors in classification. In particular, classification of VT events was affected during the stage of dome dormancy; *H* and LP events were concerned for stages of dome growth. The importance of such effects on time series was evaluated using statistical tools (cf. Section 3.4). In order to overcome these problems, an automatic method for the classification of seismic transients based on Artificial Neural Networks was proposed for Soufrière Hills by Langer et al. (2003). Since automatic classification results were not available for the entire period of interest, we have applied the data from the MVO manual classification for this study.

The cause of hybrid and long-period events are still uncertain, with recent interpretations favouring fracture development and stick-slip processes along the margins of the conduit due to flow of gas pressurised magma at depths up to 2 km (Neuberg et al., 2006-this issue, Wylie et al., 1999). Whether hybrid and long-periods really constitute two separate families or there is a continuum between these two end members is also under debate. Sometimes the same event is classified differently at different stations, but at the same time the two families apparently show different behaviour. For instance, hybrid events usually occur in swarms, while long-period habitually do not. For this work we stick to the classical MVO classification that keep these two families separate. Rockfall (RF) events reflect dome growth, although not in a simple proportional way, since rockfall activity is controlled by not only extrusion rate but also by dome size and configuration (Calder et al., 2002).

In the first dome growth stage the extrusion rate was low (<1 m^3/s) in November and December 1996 (Sparks et al., 1998) and this is reflected in low rockfall and other seismic events. Extrusion rate picked up at the end of December 1996 and continued at rates of 2–3 m^3/s, with some fluctuations related to the emplacement of distinct lobes of lava (Watts et al., 2002). This elevated activity is manifested in the increased rates of hybrid, long-period and rockfall activity (Fig. 2). The extrusion rate increased markedly in May 1997 to values of 7–8 m^3/s (Sparks et al., 1998). This period was the most vigorous of the eruption with several major dome collapses and two episodes of repetitive Vulcanian explosions in early August and then 22 September to 22 October 1997. Seismic and tilt data show that there were well-defined pulses of activity each lasting 6 to 7 weeks (Voight et al., 1999; Sparks and Young, 2002). Pulses were marked by abrupt increases in seismicity, which can be seen in the hybrid data (Fig. 2) and by major changes in the pattern of deformation recorded by tiltmeters close to the dome (Voight et al., 1999). Major dome collapses occurred within a few hours to a few days of the onset of a pulse and at the time this periodic behaviour was used by the MVO to anticipate dangerous situations.

The stage of dome dormancy was marked by much volcanic unrest (Norton et al., 2002). Several dome collapses occurred including a large (30 million m^3) collapse on 3 July 1998. 123 explosions were recorded, gas emissions continued at levels much higher than could be accounted for by residual degassing of the magma in the conduit (Edmonds et al., 2003), and ground deformation was consistent with a pressurising magma chamber at depths of 5 km or more (Norton et al., 2002). In this period VT activity was high, rates of hybrid events were negligible and long-period activity continued at a low rate (Fig. 2). Rockfall activity was also lower but continued, reflecting the instability of the remnants of the dome formed in the first stage.

The second stage of dome growth was heralded by a hybrid swarm a few weeks before the new dome appeared (Norton et al., 2002). Extrusion rate was estimated by MVO to have been in the range 2–3 m^3/s on average. In general extrusion was steadier than in

the first stage. Nevertheless seismic indicators of dome growth suggest significant fluctuations. A characteristic pattern was that hybrid earthquake swarms often occurred a few days prior to an increase in the rate of extrusion being observed. Since the direction of extrusion often changed at such times, and increased levels of dome instability (rockfall activity) soon followed, these hybrid swarms became important warning signals for MVO. For the dataset there were also some short periods of dome dormancy lasting up to several weeks and these correspond to periods of relative low long-period and hybrid event rates. In the period covered by the dataset large collapses occurred on 20 March 2000 (Carn et al., 2004) and on 29 July 2001. These collapses were followed by several weeks of lower rockfall activity as a consequence of the small size of the active dome growing in the collapse scar.

Among the complex sequences of events that have occurred during the course of the Soufrière Hills eruption, we have decided to choose the onset of the dome growth in November 1999 as event to test our probabilistic approach to forecasting. The choice of this important event was motivated by: (a) the correlated effects likely to be expressed in terms of seismic events and (b) the implications of forecasting the onset of the dome growth in relation to probabilistic risk assessments.

3.3. Statistical analysis

The calculated statistics for the different events per day and their cumulative magnitude are given in Table 1. These time series cover a period of about six years. During this period, few acquisition problems were encountered which explain the low percentage of missing values (equal to 5%) observed. The VT and *H* events present the highest coefficient of variation as well as the largest percentage of zero values. The occurrence of VT and *H* events being almost always organised in swarms explain these results.

Table 2
Linear correlation coefficients (1 November 1996 to 28 February 2003)

Time series	VT	*H*	LP	RF	VT_cm	H_cm	LP_cm	RF_cm
VT	1	−0.1	−0.1	−0.2	0.7	−0.1	−0.2	−0.2
H		1	0.1	0.0	−0.1	0.6	0.06	−0.3
LP			1	0.5	−0.2	0.1	0.7	0.4
RF				1	−0.3	0.0	0.6	0.7
VT_cm					1	−0.1	−0.3	−0.3
H_cm						1	0.1	0.1
LP_cm							1	0.6
RF_cm								1

The classical linear correlation coefficients (Priestley, 1981) were calculated for all possible pairs of time series (see Table 2). The different event occurrences present remarkable correlations (ca. 0.7) with their respective cumulative magnitude. The only other noticeable correlated pairs (greater or equal to 0.5) between different types of events are: LP–RF, LP_cm–RF and LP_cm–RF_cm. This correlation between LP and RF events could be related to specific dome activity; e.g., a flurry of LP and RF events heralding the growth of a new dome lobe.

3.4. Detection of correlation

The analysis of correlation and cross correlation in time was performed using, respectively, the variogram for individual times series and the cross variogram for pairs of time series. The variogram characterises statistically the differences between values of a time series, at distinct points in time, as the time interval separating these points increases. When correlation occurs, values taken at points at small time intervals are likely to be more similar than values taken at larger intervals in time. This persistent behaviour for a time series expresses the memory of its past activity. Characteristics of persistence are needed for a time series to be considered a potential precursor.

Table 1
Statistics for the time series (1 November 1996 to 28 February 2003)

Time series	Minimum	Maximum	Mean	Standard deviation	Variance	Coeff. of variation	Number of sampled days	Percentage of zeros
VT	0	139	2.4	6.3	40.0	2.6	2199	57
H	0	769	14.7	51.9	2690.1	3.5	2199	44
LP	0	97	5.6	8.6	73.9	1.5	2199	35
RF	0	209	44.5	44.1	1945.6	1.0	2199	1
VT_cm	0.0	4.2	0.6	0.9	0.7	1.3	2199	57
H_cm	0.0	5.1	1.1	1.2	1.3	1.1	2199	44
LP_cm	0.0	4.0	1.1	1.0	1.0	0.9	2199	35
RF_cm	0.0	5.2	2.4	0.8	0.6	0.3	2199	1

Differences in variability of event occurrences between stages of dome growth and dome dormancy were observed over the 6-year period (cf. Fig. 2). Therefore, the variograms were calculated by periods of dome growth and dome dormancy for the time series VT, *H*, LP and RF events (see Fig. 3).

During stages of dome growth, the initial (growing) behaviour of the variograms for *H*, LP and RF events were followed by a more stable part fluctuating around the variance of the data (dashed line). For the first stage of dome growth (Nov. 96 to Mar. 98), the time scale corresponding to the first stabilisation level of the variogram (around the variance) was estimated to be between 20 and 40 days for *H*, LP and RF events. These time series exhibit a persistent behaviour; i.e., the activity occurring today presents some similarity with the activity of the 3–5 weeks before. Such behaviour was not observed for VT events the variogram for which showed no remarkable initial (growing) behaviour as it starts at a much higher level in comparison to the variograms of the other events. The VT variograms are strongly dominated by a random component and only exhibit a stochastic component with a weak intensity. Therefore, the behaviour of the VT event was not considered as persistent. Variograms for the second stage of dome growth (Nov. 99 to Feb. 03), yield similar results, except for the time scale associated with the RF events which is significantly longer, at about 150 days.

The results can be interpreted in terms of two contrasting time-scales observable from geophysical data. Voight et al. (1999) observed cyclic patterns of seismicity (largely LP and H) and dome growth (causing RF signals) that had three scales of several hours (4–36 h). Also there are 6–7 weeks patterns of enhanced activity, which were especially prominent in 1997. The time scales of up to 40 days are related to this dynamical periodicity.

For the stage of dome dormancy, no structured behaviour was observed for VT, *H* and LP events. The only persistent behaviour was displayed by the RF events with a time scale between 30 and 60 days.

For the different dome stages, similar types of persistent behaviour were also detected for the time series of daily cumulative magnitude. The absence of persistent behaviour during dormancy could be related to classification problems for the VT events (cf. Section 3.1) and to the low level of seismic activity for the *H* and LP events during that period.

The calculation of cross variograms by period was performed on the basis of the largest correlation coefficients. The pairs RF–LP and LP–LP_cm events were selected due to their persistent behaviour during periods of dome growth (see Fig. 4). The time scales for the first period of dome growth were equal to approximately 20 days for the pairs RF–LP and LP–LP_cm and then these time scales increased to about 70 to 100 days for the second period of dome growth.

3.5. Precursor identification

Time series with persistent behaviour represent potential precursors. Their capability, however, needs to be evaluated in relation to forecasting specific eruptive events. Precursor identification was achieved by the direct monitoring of time series and the monitoring of parameters estimated from time series prior to the onset of dome growth in November 1999.

The *H* events constitute the only analysed time series presenting a remarkable precursory behaviour detectable by direct monitoring. After an extended period of quiescence, *H* activity has recommenced 2 to 3 weeks before the appearance of the new dome in November 1999 (cf. Fig. 2). Since the *H* events present a direct link with the volcanic activity; their time scale (estimated at ca. 20 days, cf. Section 3.4) delivers an estimate for the time elapsed between the start of *H* activity and the likelihood for the onset of the dome growth.

Monitoring changes in parameters was performed by (cross) variogram calculation using a moving window approach. Instead of calculating the (cross) variogram for the entire period of dome growth (or dormancy), it was computed by applying a moving window of 100 days along the entire time series. By estimating parameters for each (cross) variogram, the evolution of the behaviour for the time series can be monitored in terms of persistence and intensity.

This approach was applied for the RF events and the time series LP and LP_cm. In both cases, the monitored (cross) variogram parameters display behaviours with higher parameters values for period of dome growths in comparison to the period of dome dormancy (see Fig. 5). For the RF events, the calculated variogram parameter B (cf. Section 2.3) indicates the relative intensity for the stochastic component varying between 0 (random) and 1 (persistent). For the time series LP and LP_cm, the cross variogram parameter G, obtained by integration of the variogram at the window scale, delivers a measure of the overall cross variability between the time series at the window scale (cf. Section 2.3).

Both monitored parameters exhibit an upward trend occurring months before the onset of the dome growth in November 1999 (cf. Fig. 5). These

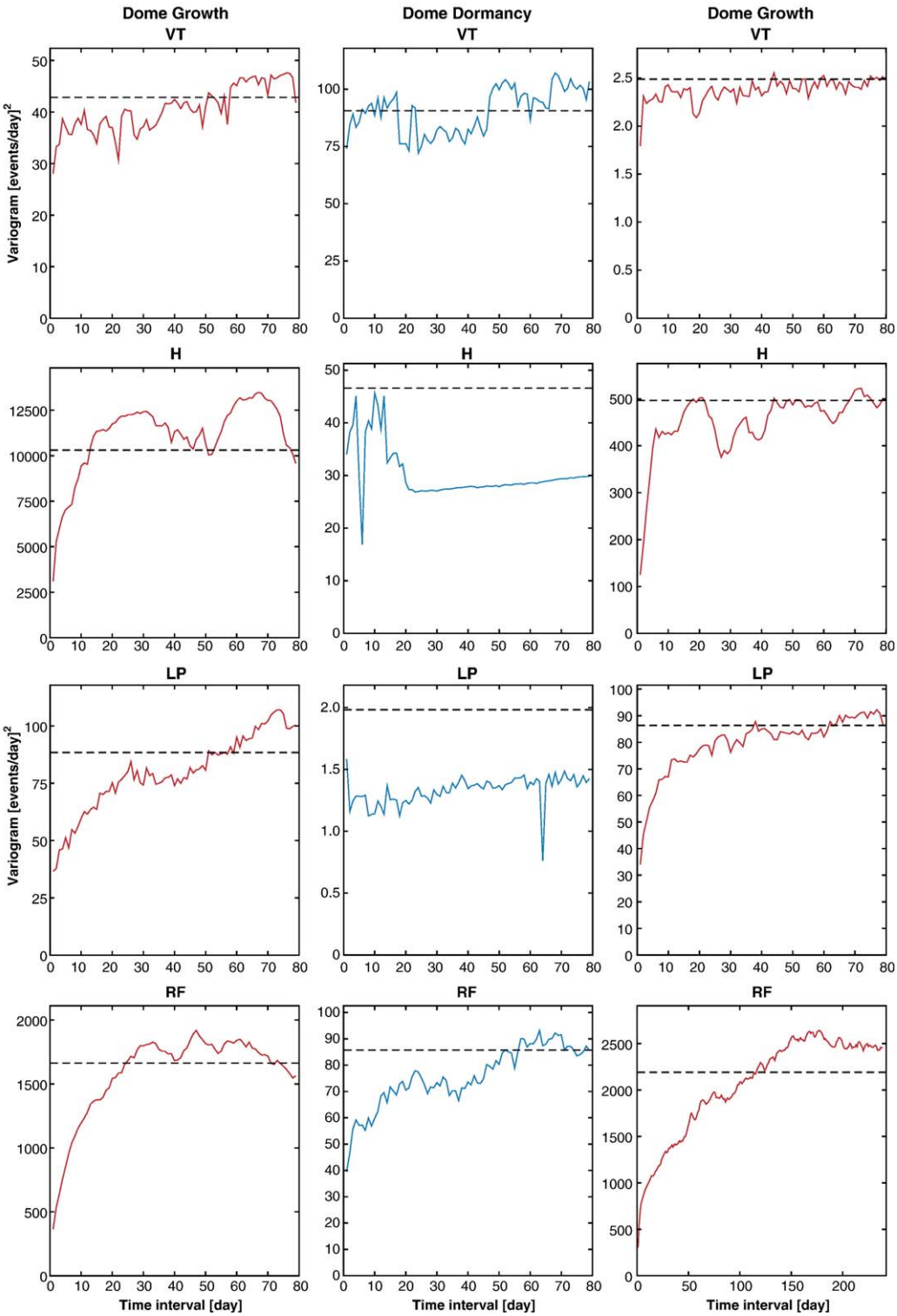

Fig. 3. Variograms for time series VT, *H*, LP and RF during episodes of dome growth Nov. 96–Mar. 98 and Nov. 99–Feb. 03) and dome dormancy (Mar. 98–Nov. 99).

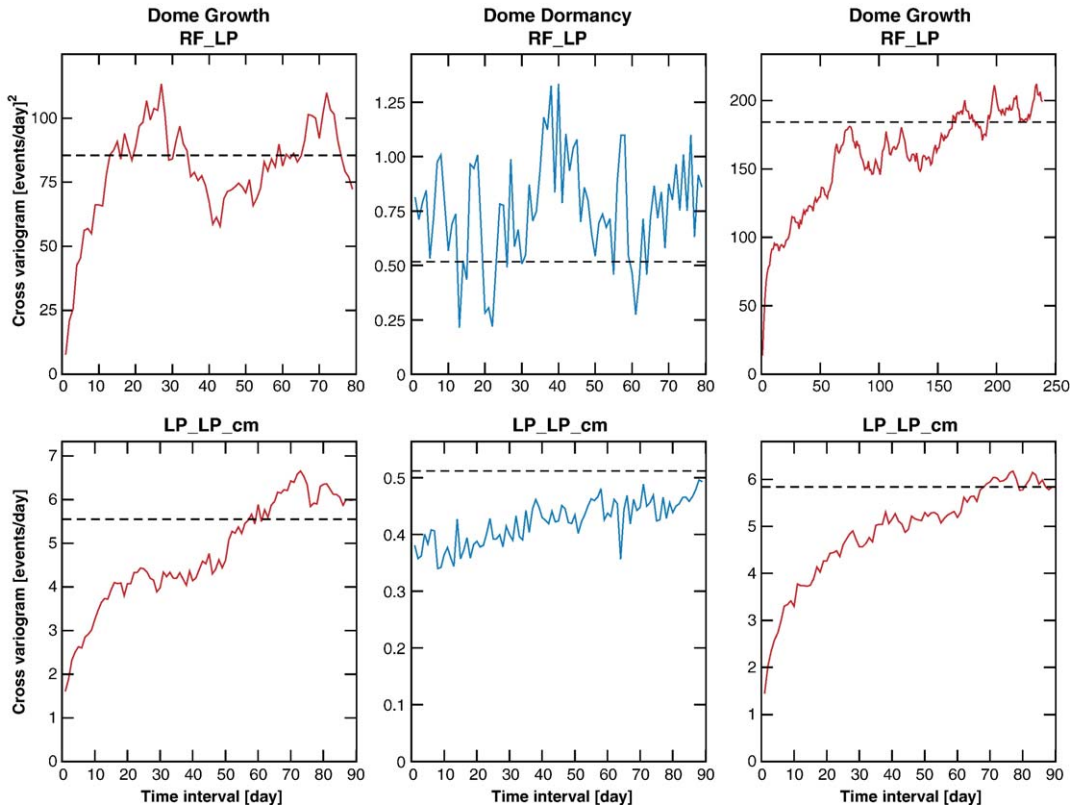

Fig. 4. Cross variograms for time series RF–LP and LP–LP_cm during episodes of dome growth Nov. 96–Mar. 98 and Nov. 99–Feb. 03) and dome dormancy (Mar. 98–Nov. 99).

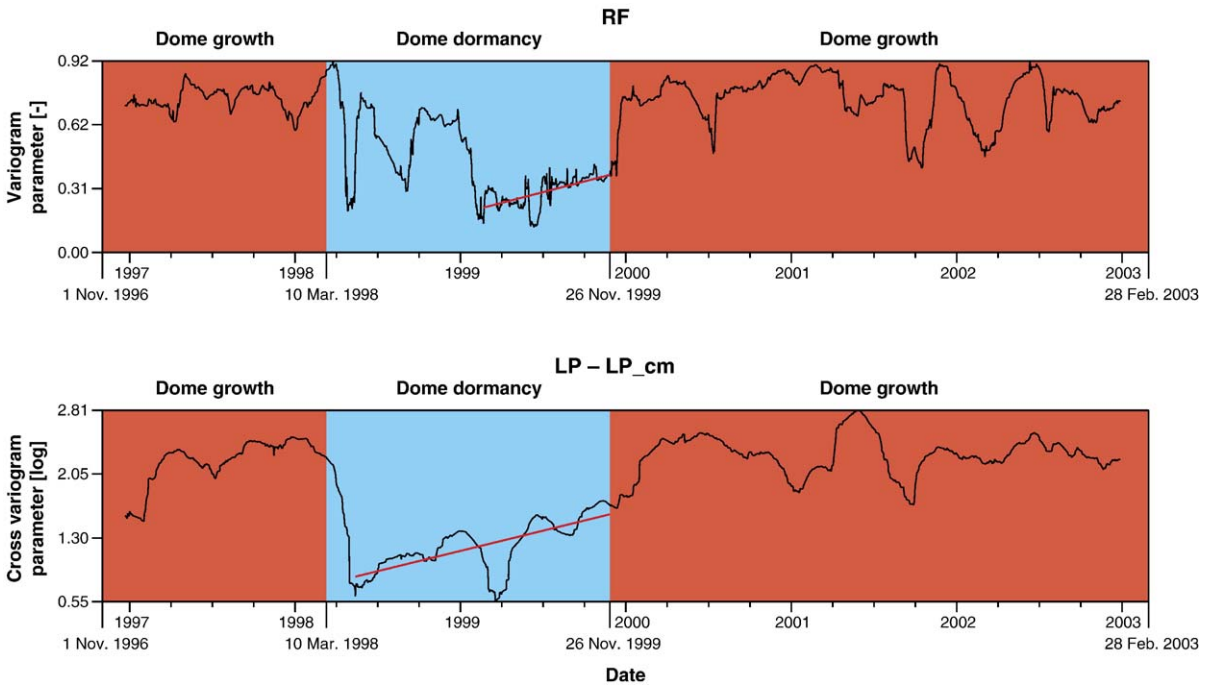

Fig. 5. Forecasting the onset of dome growth using univariate parameter monitoring estimated from rockfall events and multivariate parameter monitoring estimated from long-period events and their cumulative magnitude.

trends can be considered as precursory behaviours indicating changes in the volcanic edifice in terms of persistent behaviour for RF events as well as in terms of correlation between the time series LP and LP_cm. In other words—although we cannot obviously prove that this is the typical dynamical development for all eruptions, even of the same kind—in the analysed case as the onset of the dome growth approaches, a more structured behaviour of the volcano dynamics emerges, expressed by more persistent and correlated seismic signatures.

3.6. Stochastic forecasting

On the basis of the precursory behaviour encountered for the RF events, a period of ca. 4 months (19 July 1999 to 26 November 1999) was selected for stochastic simulation. The objective is the assessment

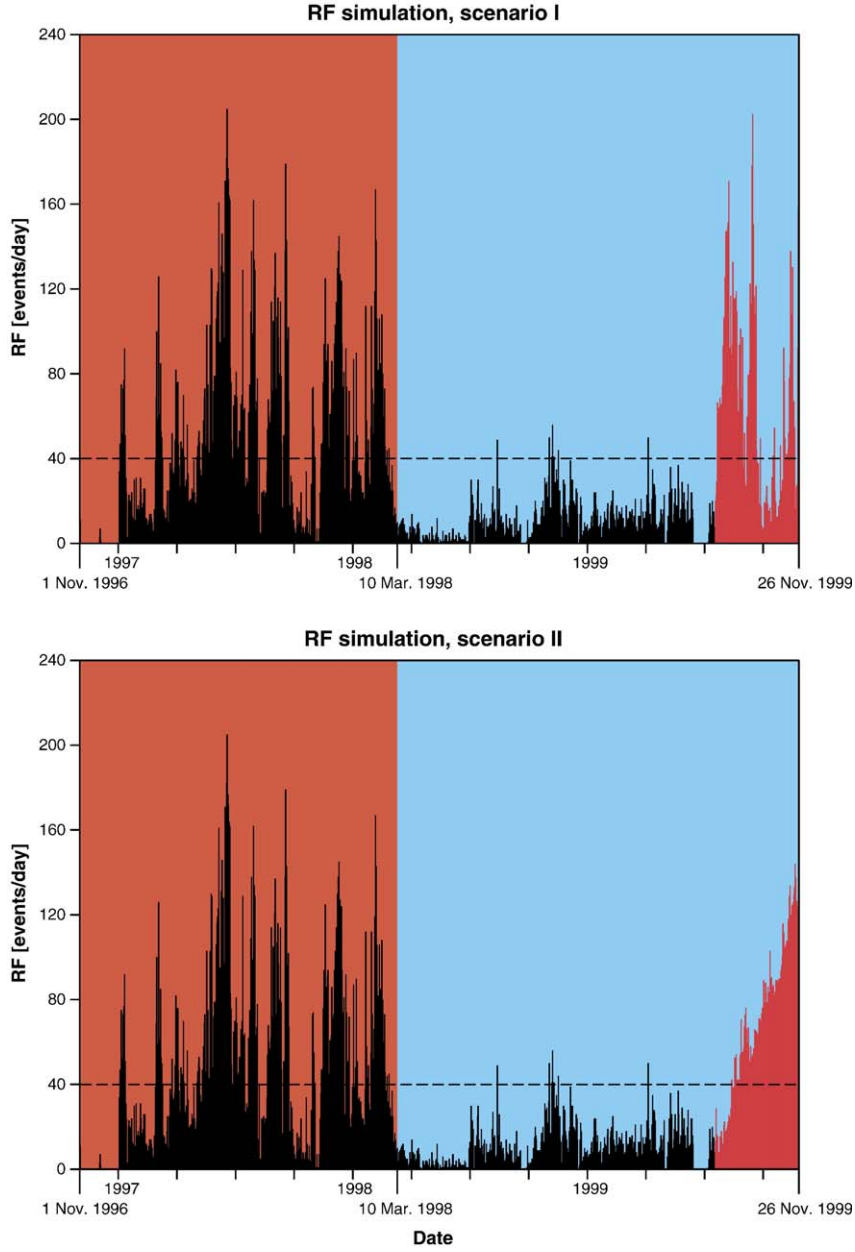

Fig. 6. Stochastic simulations (red) of rockfalls events from 19 July 1999 to 26 November 1999 for scenario I and scenario II (with drift). The horizontal (dashed) line corresponds to threshold used for estimating probability of exceedance by Monte Carlo simulations. (For interpretation of the references to colour in this figure legend, the reader is referred to the web version of this article.)

of the likelihood of the onset of dome growth for the next 4 months under the assumption that monitoring data were available up to mid-July. Since the date for the onset of dome growth is known (27 November 1999), the obtained forecasts for the chosen period can be compared to the observed reality.

Following the stage of dome dormancy, several scenarios are plausible in terms of RF activity. Simple scenarios were chosen on the basis of the observed behaviour for the RF time series: (a) scenario I with a sudden change in RF activity based on the behaviour of the first dome growth stage and (b) scenario II with a gradual (linear) change in RF activity, occurring over a 2 months period, and associated with the behaviour of the dome dormancy stage.

The median of RF events during the first stage of dome growth was selected as the threshold above which dome growth could occur. This threshold, estimated over a period of more than one year, seems an appropriate choice when comparing the variability of RF events during the stages of dome growth and dome dormancy (1 November 1996 to 26 November 1999; cf. Fig. 2).

A Monte Carlo approach was performed for the two scenarios (see Fig. 6); i.e., for each scenario 100 stochastic simulations were carried out in order to estimate probability of RF exceedance in relation to the threshold. The stochastic simulations of scenario I match the variogram and the data histogram of the stage of dome growth. For the scenario II, a linear drift was fitted between the end episode of the dome growth stage (February 1998) and the beginning episode of the dome dormancy stage (March 1998). This drift expresses the decrease in the mean number of RF events per day at a time scale of ca. 2 months (cf. Section 3.4). A similar drift (with a positive slope) was assumed to represent the increase in the mean number of RF events per day leading to a stage of dome growth. To this drift, stochastic simulations of the residual for the number of RF events per day (cf. Section 2.4) were added that matched the variogram for the stage of dome dormancy.

The results of the Monte Carlo stochastic simulations deliver estimates of exceedance probability. These estimates can be interpreted as probability of occurrence for the onset of the dome growth over a period of 4 months (Table 3). For the two scenarios, the estimated probability reveals the strong potential for the onset of dome growth which in effect has occurred end of November 1999. These estimated probabilities, reflecting the likelihood for volcanic activity, correspond to an uncertainty measure of hazard occurrence for a given period. Using these probabilities, risk analysis can then be performed with an outcome expressed in terms of life and property losses. These results lead to decision making; e.g., an evacuation could be carried out even in the presence of relatively low probabilities when the calculated risk becomes unacceptable for the population. Therefore, the selection of a hazard probability threshold is case dependent and can only be assessed through risk assessments.

4. Conclusions and perspectives

The DEVIN approach aiming at forecasting volcanic activity using stochastic methods relies on statistical analysis and direct characterisation of the behaviour of multi-parametric time series sampled at actives volcanoes. With the help of variogram and cross variogram, persistent behaviours for seismic time series were detected for Soufrière Hills Volcano. Some of these behaviours could be related to specific types of volcanic activity such as stages of dome growth and dome dormancy. By monitoring specific variograms and cross variogram parameters estimated respectively from the time series RF events; and LP events and LP_cm, precursory behaviours were identified that could indicates the onset of the dome growth for Soufrière Hills Volcano.

For forecasting activity at Soufrière Hills Volcano, *H*, LP and RF events constitute valuable pieces of information. Besides the precursory behaviour (weeks ahead) of *H* events, RF events are of special interest, because their behaviour remains persistent during the period of dome dormancy. Therefore, the parameter monitoring of RF events and their correlation with LP events are of prime importance due to their precursory behaviour of activity likely to occur at Soufrière Hills Volcano.

Table 3
Scenarios and probability of occurrences

	Dome growth	Dome dormancy	Drift	Period of [month]	Probability of forecast dome growth onset
Scenario I	Variogram (a = 37 day)[1]	–	–	4	0.57
Scenario II	–	Variogram (a = 62 day)[1]	Linear	4	0.76

[1] a: time scale.

Estimates of probability for the onset of dome growth were obtained using a Monte Carlo approach for two plausible scenarios. The probability values (obtained for a 4 months period) reflect the level of uncertainty with respect to the occurrence of potential dome activity at Soufrière Hills Volcano. These values constitute essential input for risk assessments in relation to the state of a volcano capable of a new growth stage.

By combining parameter monitoring and stochastic simulations, the DEVIN approach allows forecasts to be performed at short to medium term at active volcanoes while accounting with the associated uncertainty. The latter aspect is essential since it constitutes a major input for risk analysis studies. In particular, such valuable input can be integrated to the formalism of generalised Bayesian Belief Networks (BBN) as applied by Aspinall et al. (2003). The BBN principle constitutes an increasingly accepted approach for performing decision-making under uncertainty. Using such an approach, capable of accommodating any forecasting results (see, e.g., Aspinall et al., 2006-this issue), should constrain the range of forecast uncertainty when performing decision-making during volcanic crises.

Further DEVIN developments will include evaluating other types of multivariate parameters for monitoring time series in relation to dome stages and other volcanic events (e.g., dome collapse, Vulcanian eruptions, etc.) occurring at Soufrière Hills Volcano. In terms of forecasting, multivariate methods for stochastic simulations will be investigated in order to produce estimate of probability accounting for cross correlation between time series with potential precursory behaviour.

Acknowledgements

This work was funded by the MULTIMO project (Energy, Environment and Sustainable Development Program, EU Contract n. EVG1-CT-2000-00021). RSTJ acknowledges a Royal Society-Wolfson Merit Award.

References

Aspinall, W.P., Woo, G., Voight, B., Baxter, P.J., 2003. Evidence-based volcanology: application to eruption crises. Journal of Volcanology and Geothermal Research 128 (1–3), 273–285.

Aspinall, W.P., Carniel, R., Jaquet, O., Woo, G., Hincks, T., 2006. Using Hidden Multistate Markov models with multi-parameter volcanic data to provide empirical evidence for alert level decision-support. Journal of Volcanology and Geothermal Research 153, 112–124. doi:10.1016/j.jvolgeores.2005.08.010.

Calder, E.S., Luckett, R., Sparks, R.S.J., Voight, B., 2002. Mechanisms of lava dome instability and generation of rockfalls and pyroclastic flows at Soufrière Hills Volcano, Montserrat. In: Druitt, T.H., Kokelaar, B.P. (Eds.), The Eruption of Soufrière Hills Volcano, Montserrat, from 1995 to 1999. Geological Society, London, Memoirs vol. 21. pp. 173–190.

Carn, S.A., Watts, R.B., Thompson, G., Norton, G.E., 2004. Anatomy of a lava dome collapse: the 20 March 2000 event at Soufrière Hills Volcano, Montserrat. Journal of Volcanology and Geothermal Research 131, 241–264.

Chilès, J.P., Delfiner, P., 1999. Geostatistics: modelling spatial uncertainty. Wiley Series in Probability and Mathematical Statistics, Wiley (695 pp.).

Edmonds, M., Oppenheimer, C., Pyle, D.M., Herd, R.A., Thompson, G., 2003. SO_2 emissions from Soufrière Hills Volcano and their relationship to conduit permeability, hydrothermal interaction and degassing regime. Journal of Volcanology and Geothermal Research 124 (1), 23–43.

Jaquet, O., Carniel, R., 2001. Stochastic modelling at Stromboli: a volcano with remarkable memory. Journal of Volcanology and Geothermal Research 105, 249–262.

Jaquet, O., Carniel, R., 2003. Multivariate stochastic modelling: towards forecasts of paroxysmal phases at Stromboli. Journal of Volcanology and Geothermal Research 28, 261–271.

Kilburn, C.R.J., 2003. Multiscale fracturing as a key to forecasting volcanic eruptions. Journal of Volcanology and Geothermal Research 125, 271–289.

Kilburn, C.R.J., Voight, B., 1998. Slow fractures as eruption precursors at Soufrière Hills volcano, Montserrat. Geophysical Research Letters 25 (19), 3665–3668.

Lantuéjoul, C., 2002. Geostatistical Simulation: Models and Algorithms. Springer, 256 pp.

Langer, H., Falsaperla, S., Thompson, G., 2003. Application of artificial neural networks for the classification of the seismic transients at Soufrière Hills volcano, Montserrat. Geophysical Research Letters 30 (21), 2090, doi:10.1029/2003GL018082.

Matheron, G., 1962. Traité De Géostatistique Appliquée. Tome, vol. 1. Editions Technip, Paris, 334 pp.

Matheron, G., 1965. Les Variables Régionalisées Et Leur Estimation. Masson, Paris, 305 pp.

Marzocchi, W., Sandri, L., Gasparini, P., Newhall, C., Boschi, E., 2004. Quantifying probabilities of volcanic events: the example of volcanic hazard at Mount Vesuvius. Journal of Geophysical Research 109, B11201, doi:10.1029/2004JB003155.

Melnik, O.E., Sparks, R.S.J., 2002. Modelling of conduit flow dynamics during explosive activity at Soufrière Hills Volcano, Montserrat. In: Druitt, T.H., Kokelaar, B.P. (Eds.), The Eruption of Soufrière Hills Volcano, Montserrat, from 1995 to 1999. Geological Society, London, Memoirs, vol. 21, pp. 307–317.

Miller, A.D., Stewart, R.C., White, R.A., Luckett, R., Baptie, B.J., Aspinall, W.P., Latchman, J.L., Lynch, L.L., Voight, B., 1998. Seismicity associated with dome growth and collapse at the Soufrière Hills volcano, Montserrat. Geophysical Research Letters 25, 3401–3404.

Neuberg J., D. Green, T. Powell, L. Collier, H. Tuffen, D. Dingwell, 2006. The trigger mechanism of low-frequency seismic events on Montserrat. Journal of Volcanology and Geothermal Research. 153, 37–50. doi:10.1016/j.jvolgeores.2005.08.008

Norton, G.E., Watts, R.B., Voight, B., Mattioli, G.S., Herd, R.A., Young, S.R., Devine, J.R., Aspinall, W.P., Bonadonna, C., Baptie, B.J., Edmonds, M., Harford, C.L., Jolly, A.D., Loughlin, S.C., Luckett, R., Sparks, R.S.J., 2002. Pyroclastic flow and explosive

activity at Soufrière Hills Volcano, Montserrat, during a period of virtually no magma extrusion (March 1998 to November 1999). In: Druitt, T.H., Kokelaar, B.P. (Eds.), The Eruption of Soufrière Hills Volcano, Montserrat, from 1995 to 1999. Geological Society, London, Memoirs, vol. 21, pp. 467–481.

Newhall, C.G., Hoblitt, R.P., 2002. Constructing event trees for volcanic crises. Bulletin of Volcanology 64, 3–20.

Ortiz, R., Moreno, H., Garcia, A., Fuentealba, G., Astiz, M., Peña, P., Sanchez, N., Tárraga, M., 2003. Villarica Volcano (Chile): characteristics of volcanic tremor and forecasting of small eruptions by means of means of material failure method. Journal of Volcanology and Geothermal Research 128 (1–3), 247–259.

Priestley, M.B., 1981. Spectral Analysis and Time Series, vol. 1. Academic Press, 653 pp.

Robertson, R.E.A., Aspinall, W.P., Herd, R.A., Norton, G.E., Sparks, R.S.J., Young, S.R., 2000. The 1995–98 eruption of the Soufrière Hills Volcano, Montserrat. Philosophical Transactions of the Royal Society 358, 1619–1637.

Sandri, L., Marzocchi, W., Zaccarelli, L., 2004. A new perspective in identifying the precursory patterns of eruptions. Bulletin of Volcanology 66, 263–275.

Sparks, R.S.J., 2003. Forecasting volcanic eruptions. Earth and Planetary Sciences Letters 210, 1–15.

Sparks, R.S.J., Young, S.R., 2002. The eruption of Soufrière Hills Volcano, Montserrat: overview of scientific results. In: Druitt, T.H., Kokelaar, B.P. (Eds.), The Eruption of Soufrière Hills Volcano, Montserrat, From 1995 to 1999. Geological Society, London, Memoirs, vol. 21, pp. 45–69.

Sparks, R.S.J., Young, S.R., Barclay, J., Calder, E.S., Cole, P., Darroux, B., Davies, M.A., Druitt, T.H., Harford, C., Herd, R., James, M., Lejuene, A.M., Loughlin, S., Norton, G., Skerrit, G., Stevens, N.S., Toothill, J., Wadge, G., Watts, R., 1998. Magma production and growth of the lava dome of the Soufrière Hills Volcano, Montserrat: November 1995 to December 1997. Geophysical Research Letters 25, 3421–3424.

Voight, B., Hoblitt, R.P., Clarke, A.B., Lockhart, A.B., Miller, A.D., Lynch, L., McMahon, J., 1998. Remarkable cyclic ground deformation monitored in real time on Montserrat, and its use in eruption forecasting. Geophysical Research Letters 25 (18), 3405–3408.

Voight, B., Sparks, R.S.J., Miller, A.D., Stewart, R.C., Hoblitt, R.P., Clarke, A., Ewart, J., Aspinall, W., Baptie, B., Druitt, T.H., Herd, R., Jackson, P., Lockhart, A.B., Loughlin, S.C., Lynch, L., McMahon, J., Norton, G.E., Robertson, R., Watson, I.M., Young, S.R., 1999. Magma flow instability and cyclic activity at Soufrière Hills Volcano, Montserrat, B.W.I.. Science 283, 1138–1142.

Voight, B., Young, K.D., Hidayat, D., Subandrio, Purbawinata, M.A., Ratdomopurbo, A., Suharna, Panut, Sayudi, D.S., LaHusen, R., Marso, J., Murray, T.L., Dejean, M., Iguchi, M., Ishihara, K., 2000. Deformation and seismic precursors to dome-collapse and fountain-collapse nuées ardentes at Merapi Volcano, Java, Indonesia, 1994–1998. Journal of Volcanology and Geothermal Research 100, 261–287.

Wackernagel, H., 2003. Multivariate Geostatistics, an Introduction with Applications, third edition. Springer, 387 pp.

Watts, R.B., Herd, R.A., Sparks, R.S.J., Young, S.R., 2002. Growth patterns and emplacement of the andesite lava dome at the Soufrière Hills Volcano, Montserrat. In: Druitt, T.H., Kokelaar, B.P. (Eds.), The Eruption of the Soufrière Hills Volcano, Montserrat 1995 to 1999, Geological Society, London, Memoirs, vol. 21, pp. 115–152.

Woo, G., 1999. The Mathematics of Natural Catastrophes. Imperial College Press, London, 292 pp.

Wylie, J.J., Voight, B., Whitehead, J.A., 1999. Instability of magma flow from volatile-dependent viscosity. Science 285, 1183–1885.